LETTER

doi:10.1038/nature13546

A major advance of tropical Andean glaciers during the Antarctic cold reversal

V. Jomelli[1], V. Favier[2], M. Vuille[3], R. Braucher[4], L. Martin[5], P.-H. Blard[5], C. Colose[3], D. Brunstein[1], F. He[6], M. Khodri[7], D. L. Bourlès[4], L. Leanni[4], V. Rinterknecht[8], D. Grancher[1], B. Francou[9], J. L. Ceballos[10], H. Fonseca[11], Z. Liu[12] & B. L. Otto-Bliesner[13]

The Younger Dryas stadial, a cold event spanning 12,800 to 11,500 years ago, during the last deglaciation, is thought to coincide with the last major glacial re-advance in the tropical Andes[1]. This interpretation relies mainly on cosmic-ray exposure dating of glacial deposits. Recent studies, however, have established new production rates[2–4] for cosmogenic ^{10}Be and ^{3}He, which make it necessary to update all chronologies in this region[1,5–15] and revise our understanding of cryospheric responses to climate variability. Here we present a new ^{10}Be moraine chronology in Colombia showing that glaciers in the northern tropical Andes expanded to a larger extent during the Antarctic cold reversal (14,500 to 12,900 years ago) than during the Younger Dryas. On the basis of a homogenized chronology of all ^{10}Be and ^{3}He moraine ages across the tropical Andes, we show that this behaviour was common to the northern and southern tropical Andes. Transient simulations with a coupled global climate model suggest that the common glacier behaviour was the result of Atlantic meridional overturning circulation variability superimposed on a deglacial increase in the atmospheric carbon dioxide concentration. During the Antarctic cold reversal, glaciers advanced primarily in response to cold sea surface temperatures over much of the Southern Hemisphere. During the Younger Dryas, however, northern tropical Andes glaciers retreated owing to abrupt regional warming in response to reduced precipitation and land–surface feedbacks triggered by a weakened Atlantic meridional overturning circulation. Conversely, glacier retreat during the Younger Dryas in the southern tropical Andes occurred as a result of progressive warming, probably influenced by an increase in atmospheric carbon dioxide. Considered with evidence from mid-latitude Andean glaciers[16], our results argue for a common glacier response to cold conditions in the Antarctic cold reversal exceeding that of the Younger Dryas.

The general warming trend during deglaciation was interrupted by cooler conditions in the Southern Hemisphere during the Atlantic cold reversal (ACR). Conversely, temperature records from Greenland reveal warm conditions during the ACR (termed the Bølling–Allerød interstadial in the Northern Hemisphere), followed by the cold Younger Dryas event. The response of tropical Andean glaciers to these rapid and nonlinear climate changes remains puzzling. A recent review of published data[1] suggests that tropical Andean glaciers recorded a Younger Dryas signal, a view supported by several ^{10}Be chronologies[5,8,13,15]. However, the dating accuracy of these glacier fluctuations is questionable because ^{10}Be chronologies are affected by large uncertainties (>10%) associated with the cosmogenic production rates. This prevents unambiguous attributions of glacier response to the ACR and Younger Dryas events. Indeed, at least three scaling schemes using different sea-level, high-latitude ^{10}Be production rates were considered in establishing these chronologies. More importantly, recent calibration studies for the first time established local production rates for cosmogenic ^{3}He and ^{10}Be in the high tropical Andes[2–4]. These new developments imply that all previously published moraine ages need to be reconsidered and that the mechanisms leading to glacial advance during the ACR and Younger Dryas events warrant further investigation.

Here we present a new chronology of eight prominent moraines of the Ritacuba Negro glacier (Colombia, Sierra Nevada del Cocuy) deposited during the 'late glacial', that is, the later stages of the last deglaciation. Forty-six ^{10}Be cosmic-ray exposure (CRE) ages were obtained from boulders collected on the moraines and roches moutonnées (Fig. 1 and Methods). Analytic uncertainties on the entire set of CRE ages averaged 6 ± 6%. The Ritacuba Negro glacier chronology was compared with a recalculated data set comprising 246 published ^{10}Be and 12 ^{3}He ages (Supplementary Information) obtained from 47 moraines[1,5–15] sampled on one glacier in the northern tropical Andes (NTA) and 19 glaciers in the southern tropical Andes (STA) over the last 15 kyr. The recalculated data set was standardized using the recently revised local production rate[2] of 3.95 ± 0.18 atoms g^{-1} yr^{-1} with a time-dependent scaling and a specific Andes atmosphere model (Methods). It is important to stress that the production rate used here was calibrated at locations that are comparable in elevation and latitude ranges to the dated moraines. To assess the impact of the different scaling parameters, we report the ages using four different scaling models (Methods).

When used in combination, the new and published ages allow investigation of the following key questions, at the regional scale of the tropical Andes. (1) When did the maximum glacial extents occur over the last 15 kyr in the NTA and the STA, respectively? (2) Did the tropical Andean glaciers show a synchronous behaviour? (3) What climatic mechanisms were driving the observed glacier fluctuations?

The maximum glacial extent of Ritacuba Negro glacier during the late glacial is indicated by the outer and frontal termination moraine M18, located at 3,975 m above sea level, and dates to 13.9 ± 0.3 ^{10}Be kyr ago (n = 5) (Fig. 1; ages expressed in these units are calculated from the measured ^{10}Be concentrations). Upslope, four boulders on moraine M17 are internally consistent and yield a mean CRE age of 14.0 ± 0.3 ^{10}Be kyr. Seven samples collected on the large moraine M16 yield a mean CRE age of 13.4 ± 0.3 ^{10}Be kyr. These three moraines indicate several advances or stillstands during the ACR. Upslope from M16, a very large accumulation is composed of three small moraines: M15 formed 11.8 ± 0.2 ^{10}Be kyr ago (n = 4), at the very end of the Younger Dryas, and M14 and M13 yield respective mean CRE ages of 11.3 ± 0.1 ^{10}Be kyr (n = 9) and 11.0 ± 0.4 ^{10}Be kyr (n = 4). Two samples on a roche moutonnée confirm the chronology with a mean age of 11.1 ± 0.2 ^{10}Be kyr. M12, which is roughly 350 m upslope from M13, dates to 1.2 ± 0.1 ^{10}Be kyr

[1]Université Paris 1 Panthéon-Sorbonne, CNRS Laboratoire de Géographie Physique, 92195 Meudon, France. [2]Université Grenoble Alpes, LGGE, UMR 5183, F-38041 Grenoble, France. [3]Department of Atmospheric and Environmental Sciences, University at Albany, Albany, New York 12222, USA. [4]Aix-Marseille Université, CNRS-IRD-Collège de France, CEREGE UM34, 13545 Aix-en-Provence, France. [5]CNRS, Centre de Recherches Pétrographiques et Géochimiques, UMR 7358, Université de Lorraine, BP 20, Vandoeuvre-lès-Nancy 54501, France. [6]Center for Climatic Research, Nelson Institute for Environmental Studies, University of Wisconsin-Madison, Madison, Wisconsin 53706, USA. [7]IRD-Laboratoire d'Océanographie et du Climat: Expérimentation et Approche numérique, Université Pierre et Marie Curie, F-75252 Paris Cedex 05, France. [8]School of Geography and Geosciences Irvine Building, University of St Andrews, St Andrews KY16 9AL, UK. [9]Institut de Recherche pour le Développement, CP 9214, La Paz, Bolivia. [10]Institute for Hydrology, Meteorology and Environmental Studies, Bogota, 07603, Colombia. [11]Escuela de Ingeniería Geológica, UPTC Sede Seccional Sogamoso, Sogamoso, 152211, Colombia. [12]Center for Climatic Research and Department of Atmospheric and Oceanic Sciences, University of Wisconsin-Madison, Madison, Wisconsin 53706, USA. [13]Climate and Global Dynamics Division, National Center for Atmospheric Research, Boulder, Colorado 80305, USA.

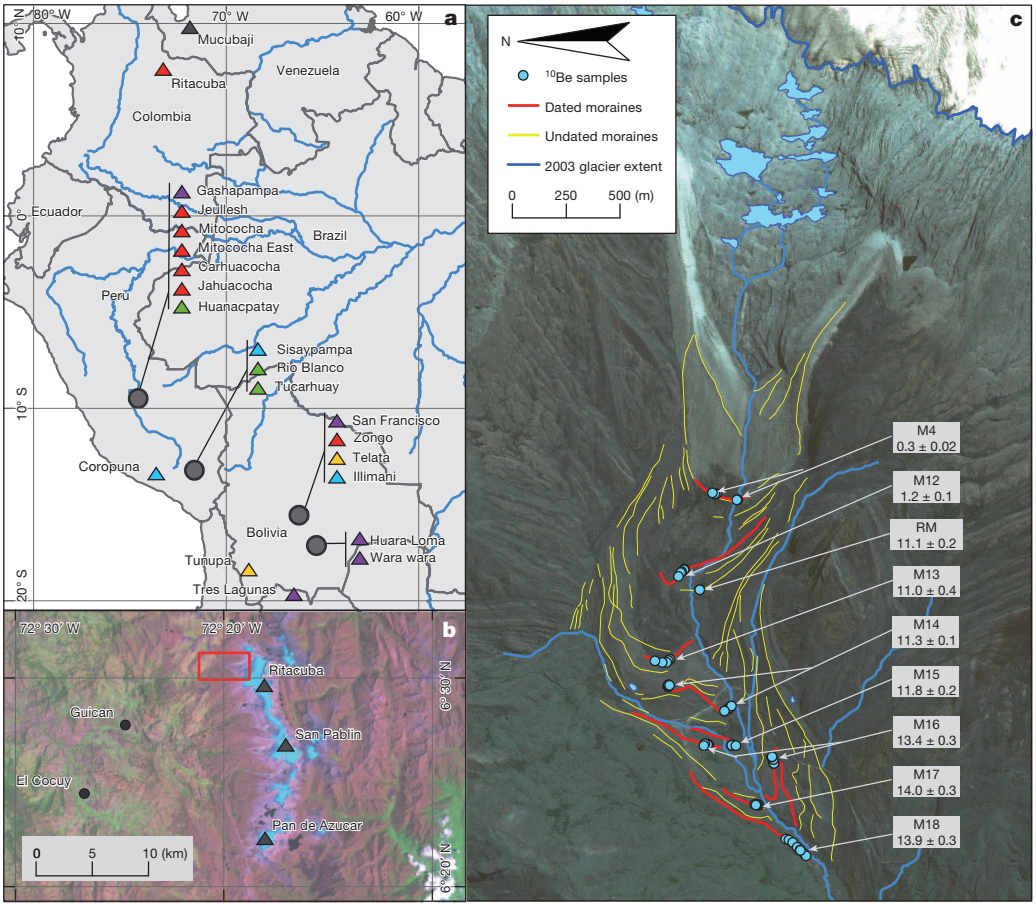

Figure 1 | The Ritacuba Negro glacier and studied sites. **a**, Location of the homogenized ^{10}Be and ^{3}He moraine record sites covering the northern and southern tropical Andes, with the largest glacial advance dated to during the ACR or possibly before (considering uncertainties) in purple; those during the ACR in red; those during the ACR or the Younger Dryas (considering uncertainties) in orange; those during the Younger Dryas in blue; those during the Holocene in green; and rejected chronology in black (Methods). **b**, Location of the northern tropical Ritacuba Negro glacial valley in the Cordillera de Cocuy (red square), with filled triangles indicating summits. **c**, Map of the Ritacuba Negro glacier, showing dated and undated moraines (prefix M indicates a main moraine as discussed in the text and RM means roche moutonnée; units, ^{10}Be kyr; Supplementary Information and Methods), the location of ^{10}Be samples (blue dots), the snout of the Ritacuba Negro glacier in 2003 (thick blue line). The uncertainties associated with the ages account for analytical uncertainties only (1 s.d.).

($n = 2$). The innermost dated moraine of the Ritacuba Negro sequence is located about 2.5 km from the present frontal position of 4,660 m above sea level. Three boulders from this ridge yield a mean CRE age of 264 ± 23 ^{10}Be yr. Finally, three small, fresh moraines were formed during the twentieth century. Among the 46 samples, six were rejected as outliers on the basis of a χ^2 test reflecting cosmogenic nuclide inheritance from previous exposures and post-depositional erosion processes (two from M18, two from M16, one from M12 and one from M4; Methods).

To evaluate the wider implications of the Ritacuba Negro glacier moraine chronology, we first compare it with indirect evidence of glacier fluctuations derived from lake-level fluctuations in Venezuela[17]. The Venezuelan glacier chronology[5] was not considered because of the uncertainties associated with ^{10}Be CRE ages (Methods). ACR advances (or stillstands) are evident in both records (moraine and lake sediments) at ~14.0 kyr ago. Minor advances (or stillstands) at the end of the Younger Dryas and during the early Holocene can also be detected in both records. However, on the basis of high titanium concentrations, ref. 17 identified a major glacial advance between ~12.8 and 12.1 kyr ago in their record. Such a glacial stillstand may have occurred in the Ritacuba Negro valley (Fig. 2), but, if so, it would necessarily have been smaller than both the ACR advances and the ones occurring at the end of the Younger Dryas. Indeed, there is no moraine dated to between 12.8 and 12.1 kyr ago preserved on Ritacuba Negro valley. However, the moraine M15, dated to 11.8 ± 0.2 kyr ago, could correspond to the end of the Younger Dryas.

We then compared the behaviour of the Ritacuba Negro glacier with 16 STA glacier chronologies that cover the ACR/Younger Dryas period (Figs 1 and 2 and Methods). The data show that seven glaciers have formed moraines at least once during the ACR chronozone *sensu stricto* and that seven others contain moraine deposits, whose dates, within the margin of error, overlap with the ACR period (Methods). Moraine formation implies the obliteration of any older moraines deposited by less extensive glaciation upstream, and the ACR advances correspond to the outermost front positions over the last 14.5 kyr in many locations in Peru, Bolivia and northern Argentina. Consequently, the corresponding ACR glacial stillstands are undoubtedly more extensive than those that occurred later during the Younger Dryas. This comparison thus reveals comparable behaviour between the Ritacuba Negro (NTA) and STA glaciers. Glacial advances during the Younger Dryas were recorded in several cordilleras but were generally slightly smaller than those occurring during the ACR. However, larger advances during the Younger Dryas than during the ACR are observed for three glaciers[9,13,15] (five within the limits of dating uncertainty; Fig. 1) and may result from site-specific conditions.

Three glaciers in our data set contain only Holocene moraines (Fig. 1 and Methods), and suggest that early Holocene glacial extents are observed in the Ritacuba valley and at many STA sites. However, it is clear that mid- and late-Holocene stillstands are very rarely observed, probably because these moraines have been erased by Little Ice Age glacial advances[18]. Hence, a coherent retreat from the ACR extent to the present

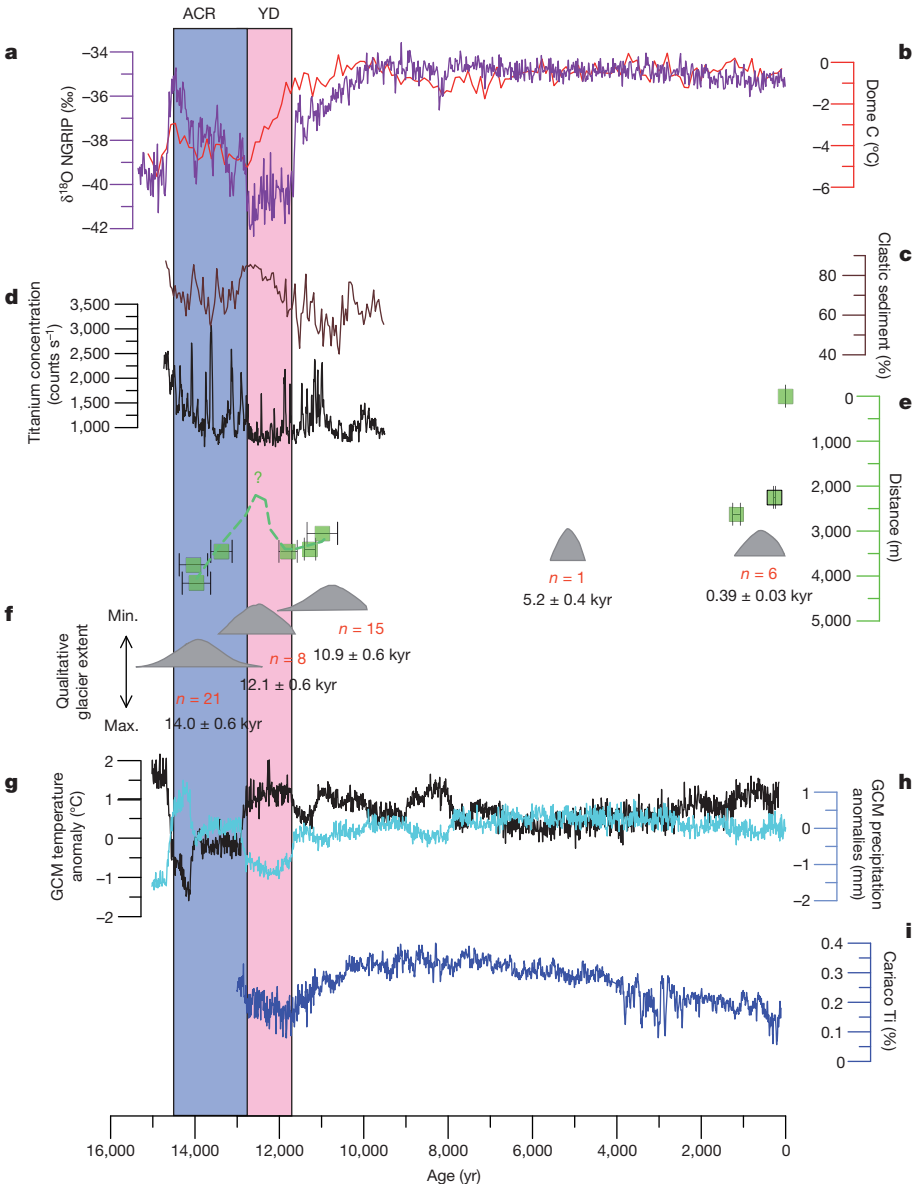

Figure 2 | Changes in the Ritacuba Negro glacier compared with proxy records. **a**, NGRIP $\delta^{18}O$ from ref. 24 (purple line). **b**, Temperature anomalies at EPICA Dome C[24] (red line). **c**, **d**, Clastic sediment (**c**; brown line) and titanium concentration (**d**; black line) from Los Anteojos lake[17] (Venezuela). **e**, Ritacuba Negro glacier front variations relative to extent in 2010 and chronology based on the 40 new ^{10}Be ages documenting the NTA region. Error bars are moraine age uncertainty (1 s.d.). The dashed line shows the possible evolution of the front. **f**, STA moraine ages (based on 246 ^{10}Be surface exposure ages from 19 glaciers; Supplementary Information and Methods). Shaded grey areas correspond to probability distribution functions of moraine ages. Their position on the *y* axis illustrates the progressive general retreat of the glaciers over time. The number of moraines <15 kyr old is shown in red, the mean age of each distribution (uncertainty, 2 s.d.) is shown in black. **g**, CCSM3 temperature anomalies in the Ritacuba region (77–69° W, 2–10° N; black line). **h**, CCSM3 precipitation anomalies in the Ritacuba region (77–69° W, 2–10° N; blue line). Anomalies are with respect to the 13.9 kyr period in the all-forcings run. **i**, Titanium concentration in Cariaco basin sediments[19]. YD, Younger Dryas; ACR, Antarctic cold reversal.

position, interrupted by minor stillstands or re-advances during the Younger Dryas and early Holocene epoch, is observed across the tropical Andes. Together these fluctuations reveal a common trend in glacier size evolution.

The glacier size evolution across the tropics during the ACR/Younger Dryas period is in step with other Southern Hemisphere glaciers such as those in Patagonia and New Zealand[16], and strongly suggests that they mostly result from a common climate driver. The fact that the NTA and STA glacier systems, each exposed to different precipitation regimes[19], display a common evolution suggests that increased temperature served as a dominant control for glacier retreat during the ACR/Younger Dryas period (Figs 2 and 3). This temperature sensitivity is consistent with modern observations which show that temperature affects glacier melt rates through a change in the rain–snow line and albedo feedbacks[20,21].

To explore possible mechanisms responsible for this tropical Andean glacier evolution during the ACR/Younger Dryas period, we analysed the transient simulation of the last deglaciation with the coupled global climate model[22] (GCM) Community Climate System Model version 3 (CCSM3) (Methods). Two studies[23,24] demonstrate that the GCM simulation successfully represents the antiphased hemispheric temperature response to ocean circulation changes during the last deglaciation. The transient simulation indicates a significant warming over the STA region during the deglaciation, interrupted by a minimum 14.1 kyr ago and a smaller decrease in temperature ~12.1 kyr ago (Fig. 3). The temperature change is in good agreement with moraine records in the STA. In the Ritacuba region, however, temperature changed rapidly between 14.1 and 11 kyr ago, with two cold episodes during the ACR and at the end of the Younger Dryas, separated by a warm period during the Younger

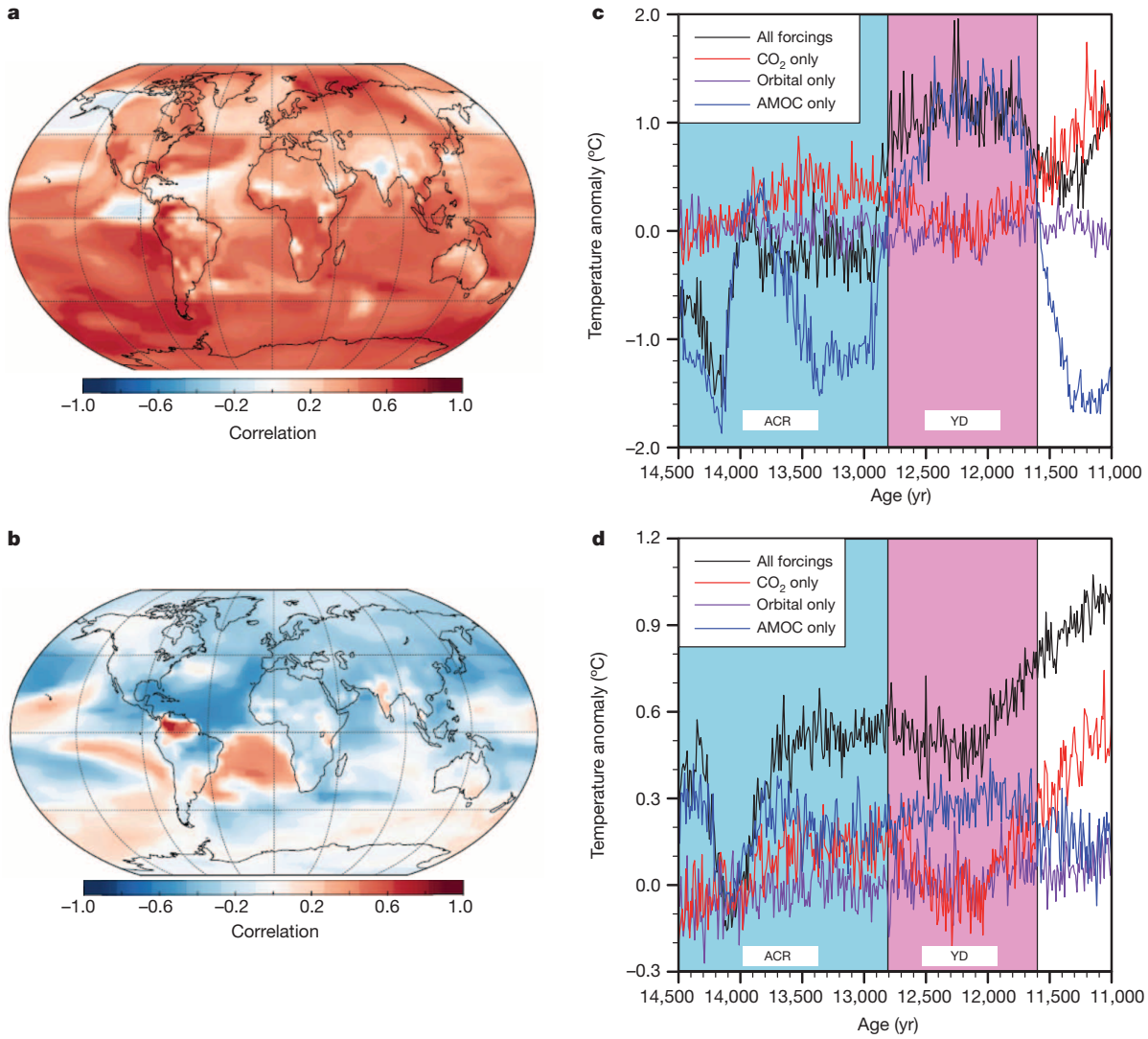

Figure 3 | Decadal temperature variations in the Ritacuba region correlated with global surface temperature. **a**, ACR period. **b**, Younger Dryas period. Statistically insignificant ($P > 0.05$) values are shown in white. **c**, **d**, Temperature evolution simulated with different CCSM3 single-forcing and all-forcing runs in the Ritacuba region (77–69° W, 2–10° N; **c**) and, documenting the STA region, in the Andes of Bolivia[14] (73–65° W, 14–22° S; **d**). The keys show the various forcings used. Anomalies are with respect to the decadal averages at 14.0 kyr in all-forcing runs.

Dryas (Figs 2 and 3). Again this temperature evolution is in agreement with our direct observations of glacier change in the Ritacuba region, but is inconsistent with results from ref. 17, where a cold episode is identified during the main Younger Dryas period on the basis of clastic sediments and pollen collected in a Venezuelan lake. This discrepancy may result from uncertainties in regional GCM simulations or from distinct sensitivities of the different proxies to climate forcing.

To further explore such a hypothesis and better understand this common glacier behaviour, decadal temperature and precipitation variations were correlated with global surface temperature and precipitation fields, respectively. During the ACR, a positive relationship is observed between temperature fluctuations in the Ritacuba region and temperatures over large parts of the Southern Hemisphere. Correlations are most significant at southern high latitudes and in the eastern equatorial Pacific (Fig. 3), with cold sea surface temperatures in the eastern equatorial Pacific being associated with glacier advance, in agreement with present-day observations[25]. During the Younger Dryas, the slowdown of the Atlantic meridional overturning circulation (AMOC) that maintained cold sea surface temperatures in the northern tropical Atlantic produced a very different pattern. In the STA, temperature evolved gradually and in step with the large-scale temperature signal. In the Ritacuba region, however, the continental temperature warmed when the cooling in the Northern Hemisphere occurred during the Younger Dryas (Supplementary Discussion). In the transient simulation, the Younger Dryas warming in the Ritacuba region results from decreased latent heat loss due to reduction of tropical forests, which is caused by the southward shift of the intertropical convergence zone[26] associated with the slowdown of the AMOC during the Younger Dryas (Supplementary Discussion and Extended Data Figs 4–9). Therefore, the temperature increase in the region during the Younger Dryas (Fig. 2) may at least in part be caused by decreased cloudiness and related local land–surface feedbacks such as reduced soil moisture and less evaporative cooling[27,28], as a result of the large-scale reorganization of precipitation over tropical South America. Other mechanisms, such as upwelling Antarctic intermediate water in the eastern tropical Pacific[29] may also have a role in NTA warming during the Younger Dryas. CCSM3 results from simulations[23] that isolate individual forcing components indicate that tropical glacier fluctuations during the ACR/Younger Dryas period were primarily driven by a CO_2 increase superimposed on AMOC variability. AMOC variability was responsible for the abrupt regional climate change observed in the NTA during the Younger Dryas period, whereas temperature changes in the STA carry a predominantly CO_2-forced fingerprint (Fig. 3).

Our results clearly demonstrate that tropical Andean glaciers were impacted by the ACR, consistent with results from recent studies in southern mid latitudes[16], suggesting a common temperature response to this event along the entire Andean cordillera. Regardless of our interpretation, any proposed mechanisms for drivers of deglacial climate change in the tropical Andes must account for the widespread stability of glacier ice during the ACR. Our analyses suggest AMOC variability superimposed on CO_2 forcing as the main drivers of the late deglaciation in the Andes. Finally, our results based on new cosmogenic production rates[2–4] illustrate that most previous chronologies and climate interpretations from tropical glaciers since the LGM may need to be revisited.

METHODS SUMMARY

To compare chronologies from the northern and southern tropical Andes, we homogenized existing late-glacial cosmogenic ^{10}Be and ^{3}He ages younger than 21 kyr (Supplementary Table 1). Beryllium-10 concentrations were normalized against an assigned value of the NIST ^{10}Be/^{9}Be ratio (2.79×10^{-11}). Existing ^{10}Be ages were recalculated using the recent Altiplano production rate of 3.95 ± 0.11 atoms $g^{-1}\,yr^{-1}$. To test the impact of the different parameters involved in the production scaling, we recalculated the age of each moraine from 20 glaciers selected in this study using four models (Supplementary Information). We excluded all glaciers that did not document the ACR–Holocene period. In this process, moraine identification was strictly the same as those documented in cited studies. We used and excluded the same samples as in the cited studies.

We did not use a χ^2 analysis to compare the ages of the moraines because such a test was not used in most previous papers. Instead, we conducted two distinct analyses on the 20 glaciers. The first was done to assess the number of glaciers with the maximum extent belonging to the ACR chronozone, assuming that the youngest moraine (as dated) since the ACR period corresponds to the maximum extent. In this case, we distinguished five different chronozones: pre-ACR, ACR, ACR/Younger Dryas, Younger Dryas and post-Younger Dryas. Each glacier was classified in a single chronozone according to the age of the maximum extent moraine and its uncertainty. The second analysis was conducted on the moraine ages to get the distribution function with time. This time we distinguished three groups of moraines, corresponding to the ACR, Younger Dryas and Holocene chronozones, respectively. Each moraine was classified in one or two distinct chronozones according to age and the associated uncertainties.

Online Content Methods, along with any additional Extended Data display items and Source Data, are available in the online version of the paper; references unique to these sections appear only in the online paper.

Received 26 November 2013; accepted 28 May 2014.
Published online 24 August 2014.

1. Rodbell, D. T., Smith, J. A. & Mark, B. G. Glaciation in the Andes during the late glacial and Holocene. *Quat. Sci. Rev.* **28,** 2165–2212 (2009).
2. Blard, P. H., Braucher, R., Lavé, J. & Bourlès, D. Cosmogenic ^{10}Be production rate calibrated against 3He in the high tropical Andes (3800–4900 m, 20–22° S). *Earth Planet. Sci. Lett.* **382,** 140–149 (2013).
3. Blard, P.-H. *et al.* Cosmogenic ^{3}He production rate in the high tropical Andes (3800 m, 20°S): implications for the local last glacial maximum. *Earth Planet. Sci. Lett.* **377–378,** 260–275 (2013).
4. Kelly, M. *et al.* A locally calibrated, late glacial ^{10}Be production rate from a low latitude, high-altitude site in the Peruvian Andes. *Quat. Geochronol.* (in the press).
5. Carcaillet, J., Angel, I., Carrillo, E., Audemard, F. A. & Beck, C. Timing of the last deglaciation in the Sierra Nevada of the Merida Andes, Venezuela. *Quat. Res.* **80,** 482–494 (2013).
6. Smith, J. A., Seltzer, G. O., Farber, D. L., Rodbell, D. T. & Finkel, R. C. Early local last glacial maximum in the tropical Andes. *Science* **308,** 678–681 (2005).
7. Zech, R., Kull, Ch., Kubik, P. W. & Veit, H. LGM and Late Glacial glacier advances in the Cordillera Real and Cochabamba (Bolivia) deduced from ^{10}Be surface exposure dating. *Clim. Past* **3,** 623–635 (2007).
8. Glasser, N. F., Clemmens, S., Schnabel, C., Fenton, C. R. & McHargue, L. Tropical glacier fluctuations in the Cordillera Blanca, Peru between 12.5 and 7.6 ka from cosmogenic ^{10}Be dating. *Quat. Sci. Rev.* **28,** 3448–3458 (2009).
9. Licciardi, J. M., Schaefer, J. M., Taggart, J. R. & Lund, D. C. Holocene glacier fluctuations in the Peruvian Andes indicate northern climate linkages. *Science* **325,** 1677–1679 (2009).
10. Hall, S. R. *et al.* Geochronology of Quaternary glaciations from the tropical Cordillera Huayhuash, Peru. *Quat. Sci. Rev.* **28,** 2991–3009 (2009).
11. Zech, J., Zech, R., Kubik, P. W. & Veit, H. Glacier and climate reconstruction at Tres Lagunas, NW Argentina, based on ^{10}Be surface exposure dating and lake sediment analyses. *Palaeogeogr. Palaeoclimatol. Palaeoecol.* **284,** 180–190 (2009).
12. Smith, J. A. & Rodbell, D. T. Cross-cutting moraines reveal evidence for North Atlantic influence on glaciers in the tropical Andes. *J. Quat. Sci.* **25,** 243–248 (2010).
13. Smith, C. A., Lowell, T. V., Owen, L. A. & Caffee, M. W. Late Quaternary glacial chronology on Nevado Illimani, Bolivia, and the implications for paleoclimatic reconstructions across the Andes. *Quat. Res.* **75,** 1–10 (2011).
14. Jomelli, V. *et al.* Irregular tropical glacier retreat over the Holocene epoch driven by progressive warming. *Nature* **474,** 196–199 (2011).
15. Bromley, G. *et al.* Glacier fluctuations in the southern Peruvian Andes during the late-glacial period, constrained with cosmogenic ^{3}He. *J. Quat. Sci.* **26,** 37–43 (2011).
16. Putnam, A. E. *et al.* Glacier advance in southern middle-latitudes during the Antarctic Cold Reversal. *Nature Geosci.* **3,** 700–704 (2010).
17. Stansell, N. D. *et al.* Abrupt Younger Dryas cooling in the northern tropics recorded in lake sediments from the Venezuelan Andes. *Earth Planet. Sci. Lett.* **293,** 154–163 (2010).
18. Jomelli, V. *et al.* Fluctuations of Andean tropical glaciers since the last millennium and palaeoclimatic implications: a review. *Palaeogeogr. Palaeoclimatol. Palaeoecol.* **281,** 269–282 (2009).
19. Haug, G. H., Hughen, K. A., Sigman, D. M., Peterson, L. C. & Röhl, U. Southward migration of the Intertropical Convergence Zone through the Holocene. *Science* **293,** 1304–1308 (2001).
20. Favier, V., Wagnon, P. & Ribstein, P. Glaciers of the outer and inner tropics: a different behaviour but a common response to climatic forcing. *Geophys. Res. Lett.* **31,** L16403 (2004).
21. Favier, V., Wagnon, P., Chazarin, J.-P., Maisincho, L. & Coudrain, A. One-year measurements of surface heat budget on the ablation zone of Antizana Glacier 15, Ecuadorian Andes. *J. Geophys. Res.* **109,** D18105 (2004).
22. Liu, Z. *et al.* Transient simulation of deglacial climate evolution with a new mechanism for Bolling-Allerod warming. *Science* **325,** 310–314 (2009).
23. He, F. *et al.* Northern Hemisphere forcing of Southern Hemisphere climate during the last deglaciation. *Nature* **494,** 81–85 (2013).
24. Shakun, J. D. *et al.* Global warming preceded by increasing carbon dioxide concentrations during the last deglaciation. *Nature* **484,** 49–54 (2012).
25. Francou, B., Vuille, M., Favier, V. & Caceres, B. New evidence for an ENSO impact on low-latitude glaciers: Antizana 15, Andes of Ecuador, 0–28°S. *J. Geophys. Res.* **109,** D18106 (2004).
26. Peterson, L. C., Haug, G. H., Hughen, K. A. & Rohl, U. Rapid changes in the hydrologic cycle of the tropical Atlantic during the last glacial. *Science* **290,** 1947–1951 (2000).
27. Leduc, G. *et al.* Moisture transport across central America as a positive feedback on abrupt climatic changes. *Nature* **445,** 908–911 (2007).
28. Davin, E. L. & de Noblet-Ducoudre, N. Climatic impact of global-scale deforestation: radiative versus nonradiative processes. *J. Clim.* **23,** 97–112 (2010).
29. Pierrehumbert, R. T. Climate change and the tropical Pacific: the sleeping dragon wakes. *Proc. Natl Acad. Sci. USA* **97,** 1355–1358 (2000).

Supplementary Information is available in the online version of the paper.

Acknowledgements Financial support was provided by the French ANR El Paso programme no. 10-blan-68-01. The ^{10}Be measurements were performed at the ASTER AMS national facility (CEREGE, Aix en Provence), which is supported by the INSU/CNRS, the French Ministry of Research and Higher Education, IRD and CEA. TRACE21 is supported by the P2C2 programme (NSF), the Abrupt Change Program (DOE), the EaSM programme (DOE) and the INCITE computing programme (DOE and NCAR). We thank M. Arnold, G. Aumaître and K. Keddadouche for their assistance during ^{10}Be measurements.

Author Contributions V.J., D.B., J.L.C. and H.F. conducted the field work on Ritacuba Negro glacier; F.H., Z.L. and B.O.-B. performed the GCM simulations; M.V. and C.C. provided temperature correlation maps; D.L.B., R.B., P.-H.B., L.L. and L.M. participated in producing the cosmogenic data; L.M., P.-H.B. and V.J. updated and homogenized the previously published cosmogenic ages; P.-H.B., V.R., V.J., D.G. and D.L.B. interpreted the cosmogenic ages; and V.J., V.F., M.V., F.H. and D.L.B. contributed to writing the paper.

Author Information Reprints and permissions information is available at www.nature.com/reprints. The authors declare no competing financial interests. Readers are welcome to comment on the online version of the paper. Correspondence and requests for materials should be addressed to V.J. (vincent.jomelli@lgp.cnrs.fr).

METHODS

The chronology of Ritacuba Negro glacier fluctuations. We report the chronology of the most complete, preserved moraine sequence from the Ritacuba Negro glacier (2.8 km^2 in 2010; 5,271 m above sea level; 6° 30′ N, 72° 20′ W), located on the western slope of the Colombian Cordillera de Cocuy. The moraines were used to estimate an earlier glacial extent and represent the minimum estimate of the fluctuations of the Ritacuba Negro glacier. The behaviour of the glacier between two successive moraine ridges is unknown. The glacier may have strongly retreated between two successive moraines observed in the field, but the front never overlapped the downslope ridge. These moraines are composed of sandstone rock blocks. Each moraine ridge was mapped by means of a differential GPS survey in the field (accuracy, <1 m; Extended Data Fig. 1). Our interpretation of moraine records is that lateral or terminal moraine ridges are constructed at times when the glacier is in, or close to, equilibrium with the prevailing climate. The reaction of the glacier in equilibrium to a superimposed climate change is almost immediate and less than the uncertainty in the dates provided in this paper. The ages provided by ^{10}Be of boulders on moraine ridges represent the onset of the retreat. Moraines are assumed to form by a combination of extreme cold situations superimposed on a long-term cold period; that is, very high-frequency (decade) cold periods superimposed on a long-term temperature minimum just before or at the beginning of a warming trend that causes glacial retreat. In other words, a moraine indicates that the glacier is beginning to retreat after reaching a maximum extent, and, hence, a moraine indicates a temperature minimum before the climate begins to warm.

The chronology of the Ritacuba Negro glacier fluctuations is based on 46 *in situ*-produced cosmogenic ^{10}Be boulder exposure ages (Supplementary Table 1 and Extended Data Figs 1–3). This chronology was based on the following considerations. Moraines are potentially vulnerable to denudation, and a moraine formed during a glacial advance is preserved and observed in the field only if the glacier did not overlap it during a subsequent extensive ice advance.

Large blocks (>60 cm high) were sampled (Supplementary Table 1) on landforms with clear geomorphologic context relating directly to a former glacier margin. Ten remains of moraine crests representing indistinguishable advances were ignored. Samples were collected from near horizontal boulder top surfaces. These boulders were preferentially collected on stable parts of the moraine crest. Denudation was considered as absent for all of them (Supplementary Table 1). We used clinometer and compass to document the surrounding topographic shielding for all sample locations. We photographed all boulders (Supplementary Information) and we measured the ground-to-sample height of every boulder (Supplementary Table 1).

Cosmic-ray exposure dating is based on the quantification of the cosmogenic nuclide content accumulated in a rock exposed at the surface to cosmic rays. This high-energy cosmic radiation induces a nuclear reaction when penetrating Earth's environment. Energetic particles interact with target atoms to produce cosmogenic nuclides. In this study, *in situ*-produced ^{10}Be was measured in the quartz mineral collected in the rock samples. Samples were crushed and sieved (250–1,000 μm); magnetic components were eliminated by means of a Frantz magnetic separator. Quartz was extracted by dissolution of unwanted minerals in mixtures of HCl and H_2SiF_6. Solutions were renewed daily until they remained clear. Potential pollution by atmospheric ^{10}Be was removed by three successive leaching steps in HF, each step dissolving ~10% of the quartz. Before complete dissolution in HF (48%), a weighted amount (~100 mg) of a 3,025 μg g^{-1} homemade ^{9}Be spike solution[30] was added. Successive separation by anion and cation exchange resins (DOWEX 1X8 then 50WX8) and precipitations were performed to isolate beryllium. The final hydroxide precipitates were dried and heated at 700 °C to obtain BeO, and were finally mixed with niobium powder to prepare targets before their measurement by accelerator mass spectrometry. All measurements were performed at the French AMS National Facility, ASTER, located at CEREGE in Aix-en-Provence. The data were calibrated directly against the National Institute of Standards and Technology (NIST) standard reference material 4325 by using an assigned ^{10}Be/^{9}Be value of $(2.79 \pm 0.03) \times 10^{-11}$ (ref. 31).

Exposure ages were calculated using a ^{10}Be production rate that has been locally calibrated in the high tropical Andes (20° S, 3,800 m) from a 15.3 ± 0.5 kyr-old surface[2,3]. Using the time-dependent scaling of ref. 32 and the specific Andes atmosphere model of ref. 33, this locally calibrated rate corresponds to a sea-level, high-latitude ^{10}Be production rate of 3.95 ± 0.18 atoms g^{-1} yr^{-1} (ref. 2). This locally calibrated production rate is based on 11 boulders, and 10 of them have cosmogenic concentrations that agree within analytical uncertainties. This low dispersion indicates that geological complications such as erosion or inheritance are not affecting this data set. This is not the case of the data set of ref. 33, which is characterized by a bimodal distribution. Although these data were used as a reference calibration site by ref. 9, we believe that the recent calibration studies by refs 2, 3 are thus more robust than those of ref. 33. Finally this rate is also in agreement with recently published independent production rate for southern Peru[4].

Time-dependent correction was done according to the model of ref. 34 and using the VDM database of ref. 35. Indeed, a recent study by ref. 36 demonstrated that atmospheric ^{10}Be records are probably the best proxy of the Earth's VDM fluctuations. Consequently, the high-resolution ^{10}Be record measured in Greenland ice[35] should be considered a more reliable estimate of the Earth's VDM than the one of ref. 37, which is used in the CRONUS online calculator[38]. This sea-level, high-latitude spallation production rate was scaled for the sampling altitudes and latitudes using the scaling factor proposed by ref. 32. To do so, a non-standard atmospheric model was used. This model takes into account the specificity of the regional atmospheric pressure according to the pressure data reported by ref. 33.

To test the impact of the scaling factors on the ages, we recalculated moraine ages using four different scaling procedures, all of them relying on the Lal/Stone polynoms[32]. Model 1 is time independent (no palaeomagnetic field correction). It considers the standard atmosphere (as defined in ref. 32). Model 2 is time independent (no palaeomagnetic field correction). It considers an alternative atmosphere model, specific to the tropical Andes (following ref. 33). Model 3 considers the time variations of production rates, using the palaeomagnetic record of ref. 35 and the geomagnetic correction described in ref. 34. The atmosphere model used is the one of ref. 32. Model 4 considers the time variations of production rates, using the palaeomagnetic record of ref. 35 and the geomagnetic correction described in ref. 34. The atmosphere model used is the tropical Andes model[33].

Given that the local calibration site used and the Ritacuba Negro moraines have nearly the same elevations and absolute latitudes, the differences between these four scaling models are limited (<5%), which strengthens the accuracy of our dating. In the main text and the figures, we have retained exposure ages calculated using model 4. This choice is justified because many data support the existence of time variations in production rates, as well as regional atmosphere peculiarities[33,36].

The calculated surface production rates were also corrected for local slope, topographic shielding due to surrounding morphologies following ref. 39, and thickness, assuming an attenuation length of 160 g cm^{-2} and a rock density of 2.7 g cm^{-3}. Analytical uncertainties (reported as 1 s.d.) include a conservative 0.5% uncertainty based on long-term measurements of standards, a 1 s.d. statistical error on counted ^{10}Be events, and the uncertainty associated with the chemical and analytical blank correction (Supplementary Table 1 and Extended Data Fig. 2).

To combine and compare the different exposure ages of Ritacuba Negro glacier, the method proposed by ref. 40 was applied (Supplementary Table 1). This method is based on χ^2 analysis. To obtain enough samples (n) per moraine, the 0.05 critical value for χ^2 with $n-1$ degrees of freedom is calculated and compared with the theoretical value given by a χ^2 table. If the calculated value is lower than the theoretical one, then all ^{10}Be ages with their analytical uncertainties are used to calculate a mean exposure age; otherwise, outliers are rejected until the distribution passes the test. Then the mean exposure age with its associated analytical uncertainty is calculated using the remaining samples (Supplementary Table 1). Analytic uncertainties for the entire set of cosmic ray exposure ages averaged 6%.

The oldest moraine in Ritacuba Negro valley, M18, is dated to 13.9 ± 0.3 ^{10}Be kyr ago on the basis of the weighted mean of five samples with their analytical standard deviation (Supplementary Table 1 and Extended Data Figs 1 and 2). Two samples, B36 and B46, dated to 15.1 ± 0.5 ^{10}Be kyr ago and 11.4 ± 0.9 ^{10}Be kyr ago, respectively, were considered as outliers on the basis of a χ^2 test reflecting isotope inheritance from previous exposure and/or post-depositional processes. Including these two samples would have given a mean value of 14.0 ± 0.2 ^{10}Be kyr.

M16 is dated to 13.4 ± 0.3 ^{10}Be kyr ago on the basis of the weighted mean of seven samples. Two samples, B30 and B33, dated to 11.4 ± 0.3 ^{10}Be kyr ago and 15.1 ± 0.6 ^{10}Be kyr ago, respectively, were rejected on the basis of the χ^2 test. Including these two samples would have given a mean value of 12.9 ± 0.2 ^{10}Be kyr.

Three hundred metres upslope, a very large lobated accumulation is composed of three younger glacial moraines from M15 to M13. M15 and M14 were dated to 11.8 ± 0.2 ^{10}Be kyr ago ($n = 4$) and 11.3 ± 0.1 ^{10}Be kyr ago ($n = 9$), respectively. Combining samples from these two moraines would have given a mean value of 11.4 ± 0.1 ^{10}Be kyr. M13 was dated to 10.9 ± 0.4 ^{10}Be kyr ago ($n = 4$).

Four small, undated recessional moraines, located only a few metres from each other and intercalated between these advanced moraines (M15–13), document numerous pulses at that time and explain the very large size of this debris accumulation.

M12 was dated to 1.1 ± 0.1 ^{10}Be kyr ago. One sample (B10), dated to 2.2 ± 0.2 ^{10}Be kyr ago, was considered an outlier on the basis of a χ^2 test reflecting isotope inheritance from previous exposure. Including this sample would have given a mean value of 1.3 ± 0.1 ^{10}Be kyr.

On M4, three boulders yielded ^{10}Be ages of 253 ± 28 yr, 263 ± 40 yr and 482 ± 130 yr, resulting in a mean age of 264 ± 23 ^{10}Be yr. A fourth boulder, dated at 1,285 ± 140 yr, was rejected. Including this sample would have given a mean value of 292 ± 22 ^{10}Be yr.

The chronology of the Andean glaciers. To compare our Ritacuba Negro record with existing chronologies from the northern and southern Andes, we compiled

and homogenized existing late-glacial cosmogenic ^{10}Be and ^{3}He chronologies (ages less than 21 kyr) from published studies from Venezuela, Peru, Bolivia and northern Argentina[1,5–15] (Supplementary Table 1). We proceeded to a homogenization (see below) of chronologies covering the last 14.5 kyr on the following bases. (1) Beryllium-10 concentrations were normalized against an assigned value of the NIST ^{10}Be/^{9}Be ratio (2.79×10^{-11}; ref. 31). Recalculations were made if necessary. (2) Existing ^{10}Be ages were recalculated using the Altiplano production rate of 3.95 ± 0.11 atoms g^{-1} yr^{-1} recently calibrated by ref. 2. All the required data for calculating the ^{3}He and ^{10}Be production rates used are available in refs 1, 2, 41. To test the impact of the different parameters involved in the production scaling, we recalculated moraine ages using the four models described above, similar to those used for the Ritacuba Negro data.

All models are shown for comparison in Supplementary Table 1, but, similarly to the Ritacuba Negro data set, we used only ages from model 4 in the figure and in the text. We then excluded all glaciers that did not document the ACR–Holocene period (for instance ref. 33) assuming that the ACR began 14.5 kyr ago.

Selected moraines for our study. Moraine identification was strictly the same as documented by other authors in their original studies. We used the same moraine notation as the authors did in their papers. When the name was missing, we arbitrary gave an alphabetic letter to each of the documented moraines, with *A* corresponding to the closest moraine from the present glacier front position. This classification was based on our analysis of maps or aerial photos shown in the papers.

We then calculated the age of each moraine. We used strictly the same samples as the authors did in their own analyses, except as regards moraine M3 from ref. 42 (Supplementary Table 1), for which we choose to differentiate the left side (dated to 14.1 ± 0.2 ^{10}Be kyr ago) from the right side (dated to 16.5 ± 0.2 ^{10}Be kyr ago). We excluded the same samples from our mean moraine age calculation as did the authors. To compare the different exposure ages of each glacial moraine, our results presented in Fig. 1 and Supplementary Table 1 were not based on a χ^2 analysis, because such a test was not used in most previous papers.

Standardized ages. We used standardized ages to retrieve glaciers with a maximum extent that occurred in the ACR to the Younger Dryas chronozone (see refs. 1, 5–15). Standardization shows that several data should be cautiously used. Ref. 43 published evidence for a Younger Dryas glacial advance in the Andes of northwestern Venezuela based on radiocarbon ages collected in Mucubají valley. Parts of these results were reinvestigated by ref. 5 using ^{10}Be CRE ages (Supplementary Table 1). However, the new local production rate incorporates the fact that on Los Zepa glacier the moraine previously attributed to the Younger Dryas by refs 43, 5 is actually older than the ACR period. On Mucubají glacier, moraine chronology shows that the level-7 frontal position corresponds to the ACR. However, we did not consider this chronology because of too large uncertainties and discrepancies with the stratigraphic order. Indeed levels 9–10 show evidence of glacial advance during the Younger Dryas. However, these ages are bracketed by two other ages that make the whole chronology questionable. Age at level 8 located at a lower altitude must be older than level 9 (considering the stratigraphic order) but shows a very large uncertainty and may correspond to the ACR–Holocene period. Age at level 11 located at the highest altitude corresponds to the ACR period but does not respect the stratigraphic order. This Venezuelan glacier was then rejected from our analysis because of too large uncertainties in the chronology.

Analysis on the retreat chronology. We then conducted two distinct analyses on the 20 glaciers.

The first one was done to assess the number of glaciers with a maximum extent belonging to the ACR chronozone. In this case, we distinguished five different chronozones: pre-ACR, ACR, ACR/Younger Dryas, Younger Dryas and post-Younger Dryas. Each glacier was classified in a single chronozone according to the age of the maximum-extent moraine and its uncertainty. To determine whether glaciers were sensitive to the ACR signal, we next counted the number of cases per group. We concluded that most glaciers were larger during the ACR than during the Younger Dryas (Supplementary Table 1). This information is given in Fig. 1.

The second analysis was conducted on the moraine ages to get the distribution function of moraines ages with time. We distinguished, this time, three groups of moraines corresponding to the ACR, Younger Dryas and Holocene chronozones, respectively. Each moraine was classified in one or two distinct chronozones according to age and the associated uncertainties. Depending on the uncertainty range, a moraine may be unequivocally attributed to one group, or the moraine age may overlap two periods, leading the moraine to be included in two groups. We next computed a density function (Fig. 2f) for those moraines associated with a specific chronozone.

Analysis of glaciers. We assumed that the youngest moraine (as dated) since the ACR period corresponds to the maximum extent of the 20 glaciers in this study. To assess whether the glacier reached its maximum extent in the ACR or in a more recent period, we classified the 20 glaciers according to the five groups presented earlier, on the basis that a glacier cannot belong to two different groups (Fig. 1).

The first group corresponds to glaciers with a maximum extent possibly included in the ACR or older (pre-ACR) if we account for the uncertainty range. Glacier Gashapampa, with a moraine dated to 14.4 ± 0.2 ^{10}Be kyr ago (purple triangle in Fig. 1), is an example.

A glacier was attributed to the second group (ACR) if the age of the maximum-extent moraine belongs to the chronozone *sensu stricto* (14.5–12.9 kyr). The term *sensu stricto* means here that the age of the moraine with the uncertainties is inside the chronozone. Jeullesh glacier is a good example, with the maximum extent moraine over the period considered dated to 13.9 ± 0.2 ^{10}Be kyr ago (red triangles in Fig. 1).

The third group corresponds to glaciers with a maximum that could be dated to the ACR or to the Younger Dryas period taking into account uncertainties associated with the age. Telata glacier, the oldest moraine of which is dated to 13.0 ± 0.7 ^{10}Be kyr ago (orange triangle in Fig. 1) is an example.

The fourth group corresponds to glaciers with a maximum extent during the Younger Dryas (*sensu stricto* 12.8–11.5 kyr ago) (blue triangles in Fig. 1).

The last group includes glaciers for which the oldest documented moraines are younger than 11.6 kyr (green triangles in Fig. 1).

Assuming this selection, 17 glaciers have a dated maximum extent during the pre-ACR/Younger Dryas period. Seventy per cent of the latter glaciers showed a maximum during the pre-ACR and ACR periods, and 30% during the Younger Dryas. Moraines of three other glaciers covered the Holocene only.

Analysis of moraines. Density functions in Fig. 2 show the distribution of moraine ages for three periods: the ACR, Younger Dryas and Holocene chronozones. Each density function is based on the number of moraines with ages belonging to the same chronozone (not the number of glaciers), taking into account that some moraines in this analysis were counted in two chronozones because we were not able to assess whether they were from the ACR or from the Younger Dryas, for instance when accounting for age uncertainties. For example, a moraine dated to 12.6 ± 1.0 ^{10}Be kyr ago was used to plot the density functions of the ACR and the Younger Dryas as well. This calculation differs from the analysis conducted on glaciers as follows. We took into account all moraines and not exclusively the largest maximum extent, and a moraine may be counted twice. Consequently, we did not focus on the number of moraines per period but focused here on the mean age and the shape of the distribution.

The moraine analysis shows that glaciers were reduced in size throughout the whole ACR/Little Ice Age period. This information is given by the position of the density function along a qualitative *y* axis, shown in grey in Fig. 2f.

A common trend in glacier size evolution. We considered glaciers to have a common glacier size evolution in the NTA and STA, on the basis of the following facts: 70% of the selected glaciers from both the NTA and the STA showed a larger advance during the ACR than the Younger Dryas; an early Holocene period characterized by moraines smaller than those characterizing the ACR/Younger Dryas period but larger than those characterizing the Little Ice Age for all glaciers; mid and late Holocene stillstands are very rarely observed (only one glacier); Little Ice Age moraines are located several hundred metres downslope from the current front position in every case.

This common trend was, however, caused by different climate drivers during the ACR/Younger Dryas period.

The coupled climate model and experimental set-up. The CGCM employed is the National Center for Atmospheric Research (NCAR) CCSM3 with a dynamic global vegetation module. CCSM3 is a global, coupled ocean/atmosphere/sea-ice/land-surface climate model without flux adjustment[44]. All the simulations were performed in the version with T31_gx3v5 resolution[45]. The atmospheric model is the Community Atmospheric Model 3 (CAM3) with 26 hybrid coordinate levels in the vertical and $\sim 3.75^{\circ}$ resolution in the horizontal. The land model uses the same resolution as the atmosphere, and each grid box includes a hierarchy of land units, soil columns and plant types. Glaciers, lakes, wetlands, urban areas and vegetated regions can be specified in the land units. The ocean model is the NCAR implementation of the Parallel Ocean Program (POP) in the vertical *z*-coordinate with 25 levels. The longitudinal resolution is 3.6° and the latitudinal resolution is variable, with finer resolution near the equator ($\sim 0.9^{\circ}$). The sea-ice model is the NCAR Community Sea Ice Model (CSIM). CSIM is a dynamic thermodynamic model that includes a subgrid-scale ice-thickness distribution. The resolution of CSIM is identical to that of POP. The preindustrial control simulation reproduces the major features of global climate, notably in the deep ocean[46]. The transient simulation was started at the end of an equilibrium run at 22 kyr. The transient concentrations of the greenhouse gases (CO_2, CH_4 and N_2O) were adopted from ref. 47. The continental ice sheets were modified approximately once per thousand years according to the ICE-5G reconstruction[48]. The coastlines at LGM were also taken from the ICE-5G reconstruction and were changed twice, at 12.9 kyr and 6 kyr. The meltwater flux was constructed roughly following the observations. More detailed discussions on the setup of this simulation can be found in refs 22, 49.

Discussion. To explore the relationship between glaciers in the STA region and climate forcing, we analysed the correlation field between temperature estimated from the model in the Andes of Bolivia[14] and global temperature (Extended Data Fig. 4). In the STA region, a significant correlation ($P < 0.05$) with Southern Hemisphere high-latitude temperature and with the Ritacuba region is observed during the ACR period. During the Younger Dryas period, the correlation with Southern Hemisphere high-latitude temperature is weaker but still significant in the tropics. The insignificant correlation on the decadal timescale between the Ritacuba region and the Andes of Bolivia can be explained by contrasting temperature variations between the two regions during this period (Fig. 3c, d).

We also computed a map of the simulated precipitation difference between the ACR and the Younger Dryas (Extended Data Fig. 5). This map shows a strong decrease in precipitation over a band that stretches from the eastern equatorial Pacific to the Caribbean, including the Ritacuba region. This figure needs to be compared with the map of temperature differences (Extended Data Fig. 4). During the ACR, a global cooling is observed in agreement with the large glacial extent in the Andes. During the Younger Dryas, however, the global temperature signal resembles the typical hemispheric see-saw. A strong increase in temperature is observed over the Ritacuba region, while the North Atlantic is anomalously cold. This pattern is confirmed by the negative correlation of Ritacuba temperature with temperature along the same areas during both the ACR and the Younger Dryas (Fig. 3). This suggests that precipitation and temperature are anticorrelated on a regional scale over the continent, a phenomenon that is also visible in Fig. 2.

In addition, analysis of the transient simulation shows that NTA warming is the result of vegetation feedback. We have included the simulated changes in precipitation (Extended Data Fig. 5), tree fraction, latent heat flux and surface temperature changes during the Younger Dryas (Extended Data Figs 6–9). These figures clearly document the following mechanism for the NTA warming. The slowdown of the AMOC induces a southward shift of the intertropical convergence zone, producing a precipitation reduction in the NTA. The resulting drought conditions lead to reduced tropical forest cover, reduced evapotranspiration and latent heat release, and consequently induces warming over the NTA. The surface warming due to reduced tree cover in the tropics is a robust result in the land cover change literature[28,50].

Finally, ref. 51 emphasized the role of CO_2 as a major driver in glacier fluctuations. Here we show that CO_2 forcing alone cannot explain the observed change in glacier extent. Transient simulations with the coupled global climate model suggest that the common glacier behaviour was the result of AMOC variability superimposed on deglacial CO_2 rise.

30. Merchel, S. *et al.* Towards more precise ^{10}Be and ^{36}Cl data from measurements at the 10^{-14} level: Influence of sample preparation. *Nucl. Instrum. Methods Phys. Res. B* **266,** 4921–4926 (2008).
31. Nishiizumi, K. *et al.* Absolute calibration of ^{10}Be AMS standards. *Nucl. Instrum. Methods Phys. Res. B* **258,** 403–413 (2007).
32. Stone, J. O. Air pressure and cosmogenic isotope production. *J. Geophys. Res.* **105,** 23753–23759 (2000).
33. Farber, D. L., Hancock, G. S., Finkel, R. C. & Rodbell, D. T. The age and extent of tropical alpine glaciation in the Cordillera Blanca, Peru. *J. Quat. Sci.* **20,** 759–776 (2005).
34. Nishiizumi, K. *et al.* Cosmic-ray production rates of ^{10}Be and ^{26}Al in quartz from glacially polished rocks. *J. Geophys. Res.* **94,** 17907–17915 (1989).
35. Muscheler, R., Beer, R., Kubik, P. W. & Synal, H. A. Geomagnetic field intensity during the last 60,000 years based on Be-10 and Cl-36 from the Summit ice cores and C-14. *Quat. Sci. Rev.* **24,** 1849–1860 (2005).
36. Ménabréaz, L., Bourles, D. L. & Thouveny, N. Amplitude and timing of the Laschamp geomagnetic dipole low from the global atmospheric ^{10}Be overproduction: contribution of authigenic ^{10}Be/^{9}Be ratios in west equatorial Pacific sediments. *J. Geophys. Res.* **117,** B11101 (2012).
37. Guyodo, Y. & Valet, J. P. Global changes in intensity of the Earth's magnetic field during the past 800 kyr. *Nature* **399,** 249–252 (1999).
38. Balco, G., Stone, J. O., Lifton, N. A. & Dunai, T. J. A complete and easily accessible means of calculating surface exposure ages or erosion rates from ^{10}Be and ^{26}Al measurements. *Quat. Geo.* **3,** 174–195 (2008).
39. Dunne, J., Elmore, D. & Muzikar, P. Scaling factors for the rates of production of cosmogenic nuclides for geometric shielding and attenuation at depth on sloped surfaces. *Geomorphology* **27,** 3–11 (1999).
40. Ward, G. K. & Wilson, S. R. Procedures for comparing and combining radiocarbon age determinations: a critique. *Archaeometry* **20,** 19–31 (1978).
41. Blard, P. H. *et al.* Progressive glacial retreat in the Southern Altiplano (Uturuncu volcano, 22°S) between 65 and 14 ka constrained by cosmogenic 3He dating. *Quat. Res.* (in the press).
42. Smith, J. A. & Rodbell, D. T. Cross-cutting moraines reveal evidence for North Atlantic influence on glaciers in the tropical Andes. *J. Quat Sci.* **25,** 243–248 (2010).
43. Mahaney, W. C. *et al.* Evidence for a Younger Dryas glacial advance in the Andes of northwestern Venezuela. *Geomorphology* **96,** 199–211 (2008).
44. Collins, W. D. *et al.* The Community Climate System Model Version 3 (CCSM3). *J. Clim.* **19,** 2122–2143 (2006).
45. Yeager, S. G., Shields, C. A., Large, W. & Hack, J. The low-resolution CCSM3. *J. Clim.* **19,** 2545–2566 (2006).
46. Otto-Bliesner, B. L. *et al.* Last glacial maximum and Holocene climate in CCSM3. *J. Clim.* **19,** 2526–2544 (2006).
47. Joos, F. & Spahni, R. Rates of change in natural and anthropogenic radiative forcing over the past 20,000 years. *Proc. Natl Acad. Sci. USA* **105,** 1425–1430 (2008).
48. Peltier, W. R. Global glacial isostasy and the surface of the ice-age. *Annu. Rev. Earth Planet. Sci.* **32,** 111–149 (2004).
49. He, F. *Simulating Transient Climate Evolution of the Last Deglaciation with CCSM3*. PhD thesis, Univ. Wisconsin-Madison (2011).
50. He, F. *et al.* Simulating global and local surface temperature changes due to Holocene anthropogenic land cover change. *Geophys. Res. Lett.* **41,** 623–631 (2014).
51. Broecker, W. *What Drives Glacier Cycles?* (Eldidgio, 2013).

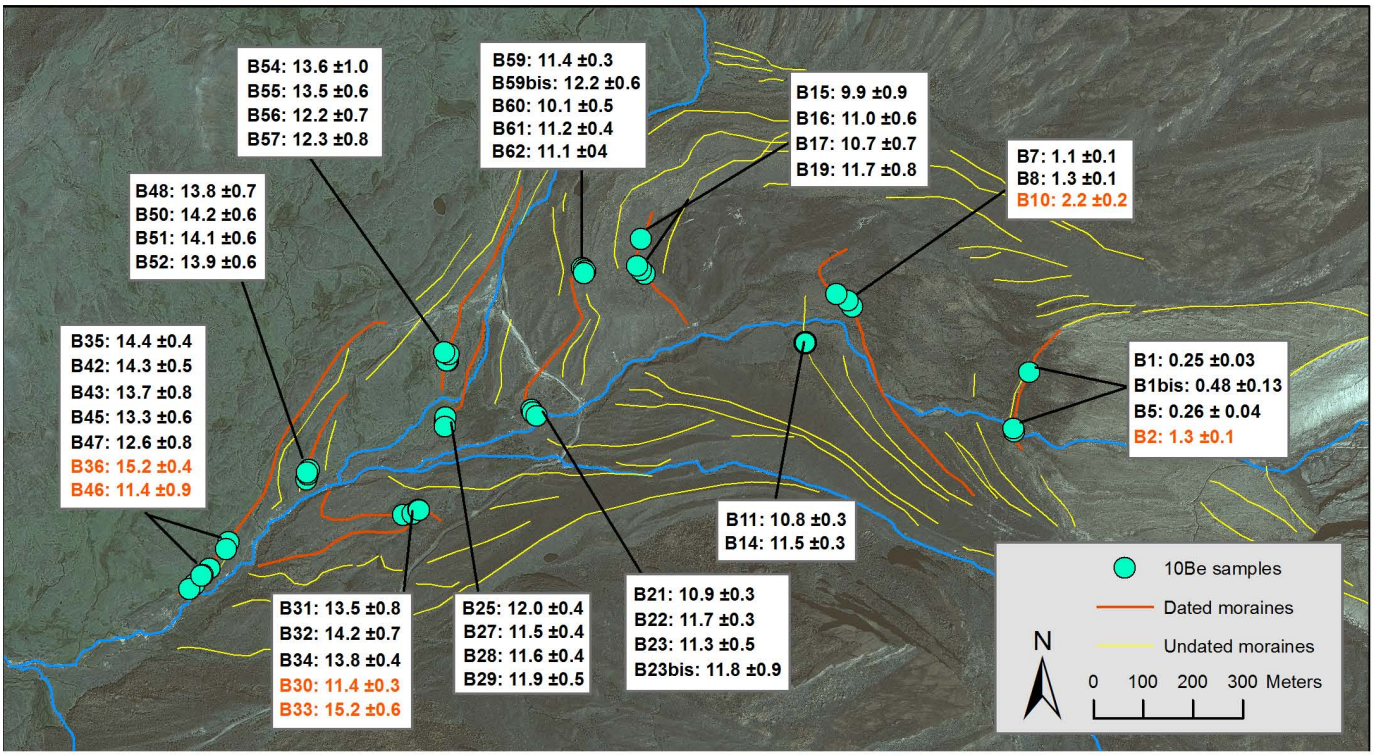

Extended Data Figure 1 | Location of the ^{10}Be samples collected on the Ritacuba Negro glacier. Rejected samples in red. Dates are given in kyr with analytical uncertainties reported as 1 s.d. Photographs of ^{10}Be sampled boulders are given in a separate file (Supplementary Information).

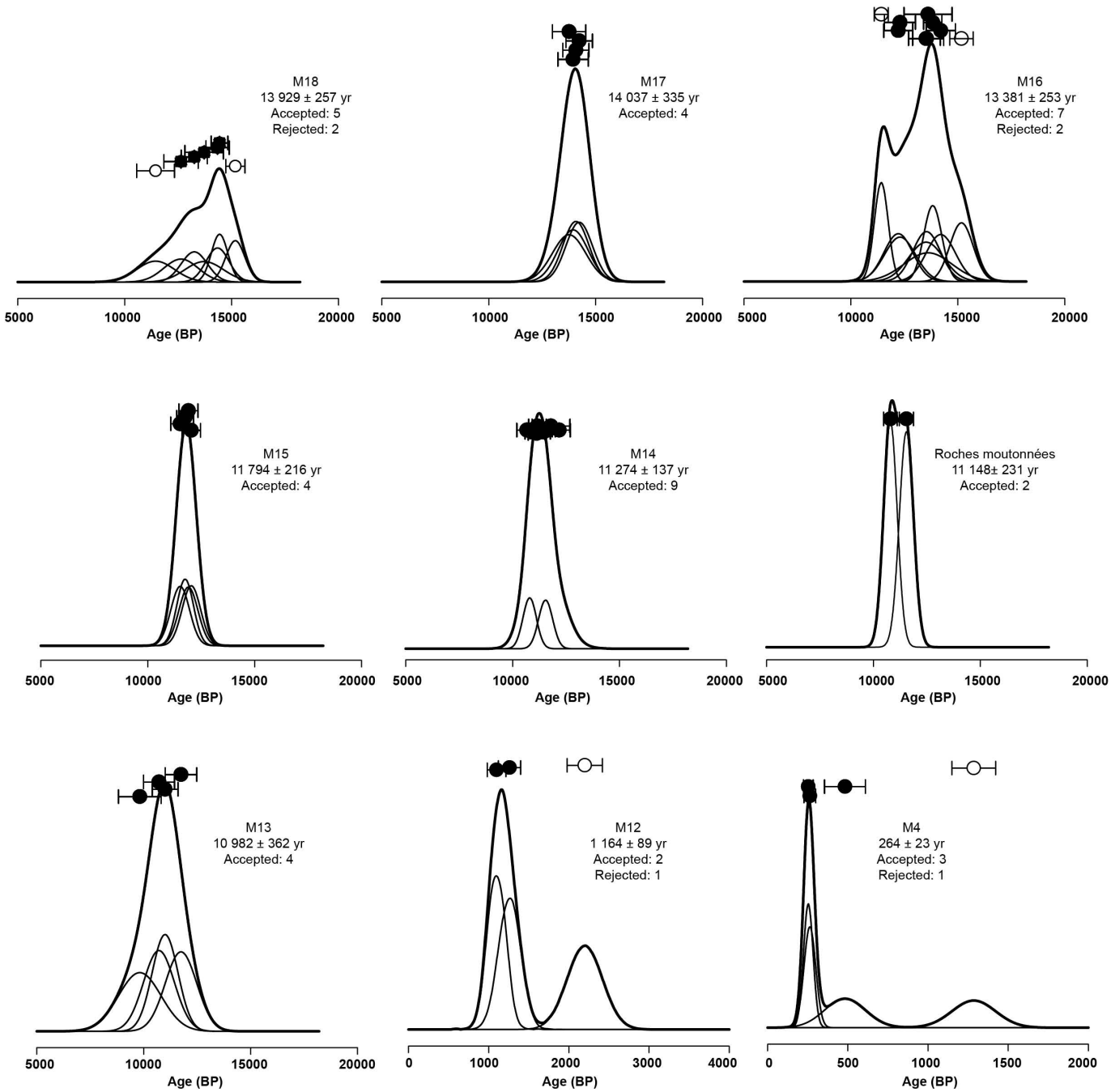

Extended Data Figure 2 | Cosmogenic ^{10}Be surface exposure ages of moraine boulders of Ritacuba Negro glacier. Error bars on each symbol represent 1 s.d. analytical uncertainty only. Open symbols indicate outliers not included in the means. Thin black curves show relative probability distributions of individual ages and thick black curves represent the cumulative probability distributions of age populations. Uncertainties associated with the mean ages account for analytical uncertainties only.

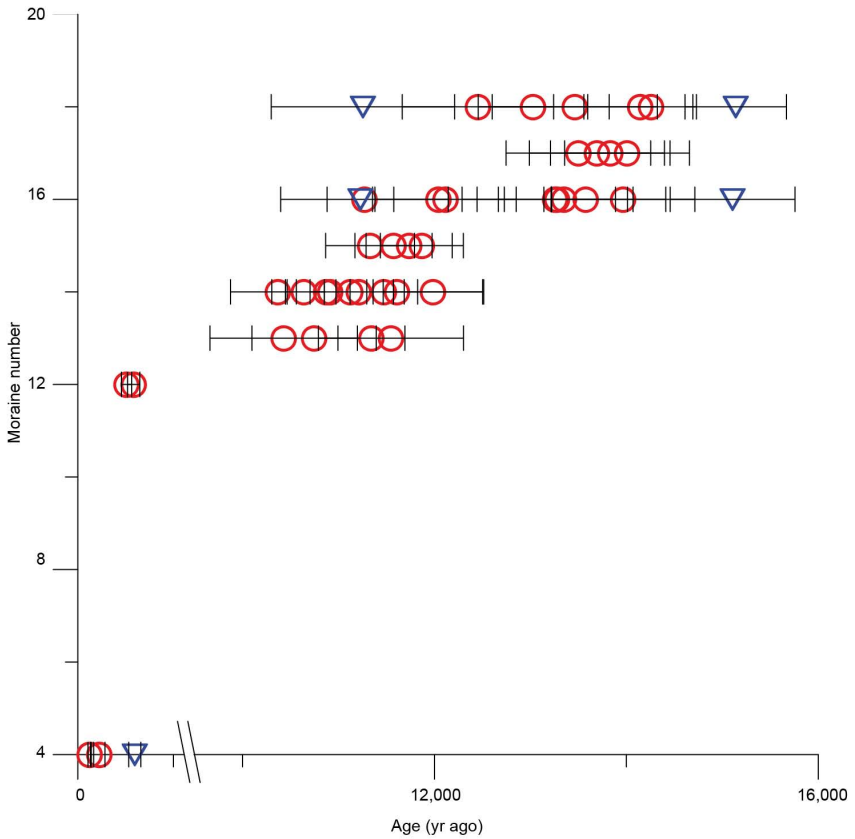

Extended Data Figure 3 | Age of the moraine versus moraine number. Error bars on each symbol represent the analytical uncertainties. Red circles indicate samples used in this study; blue triangles indicate rejected samples.

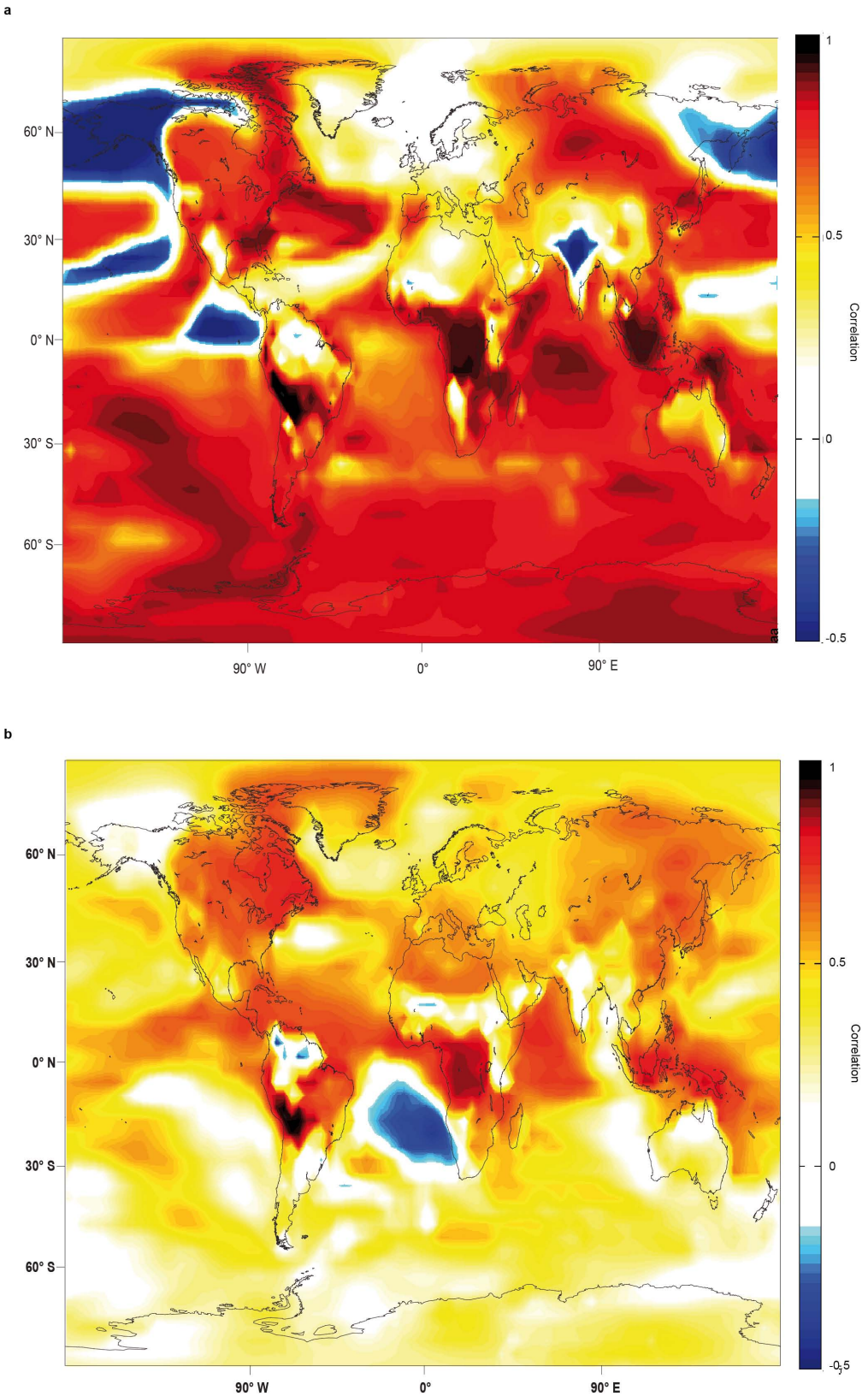

Extended Data Figure 4 | Decadal temperature variations in the Andes of Bolivia (73–65° W, 14–22° S) correlated with global temperature. **a**, Correlations during the ACR period. **b**, Correlations during the Younger Dryas period. Statistically insignificant ($P > 0.05$) values are shown in white.

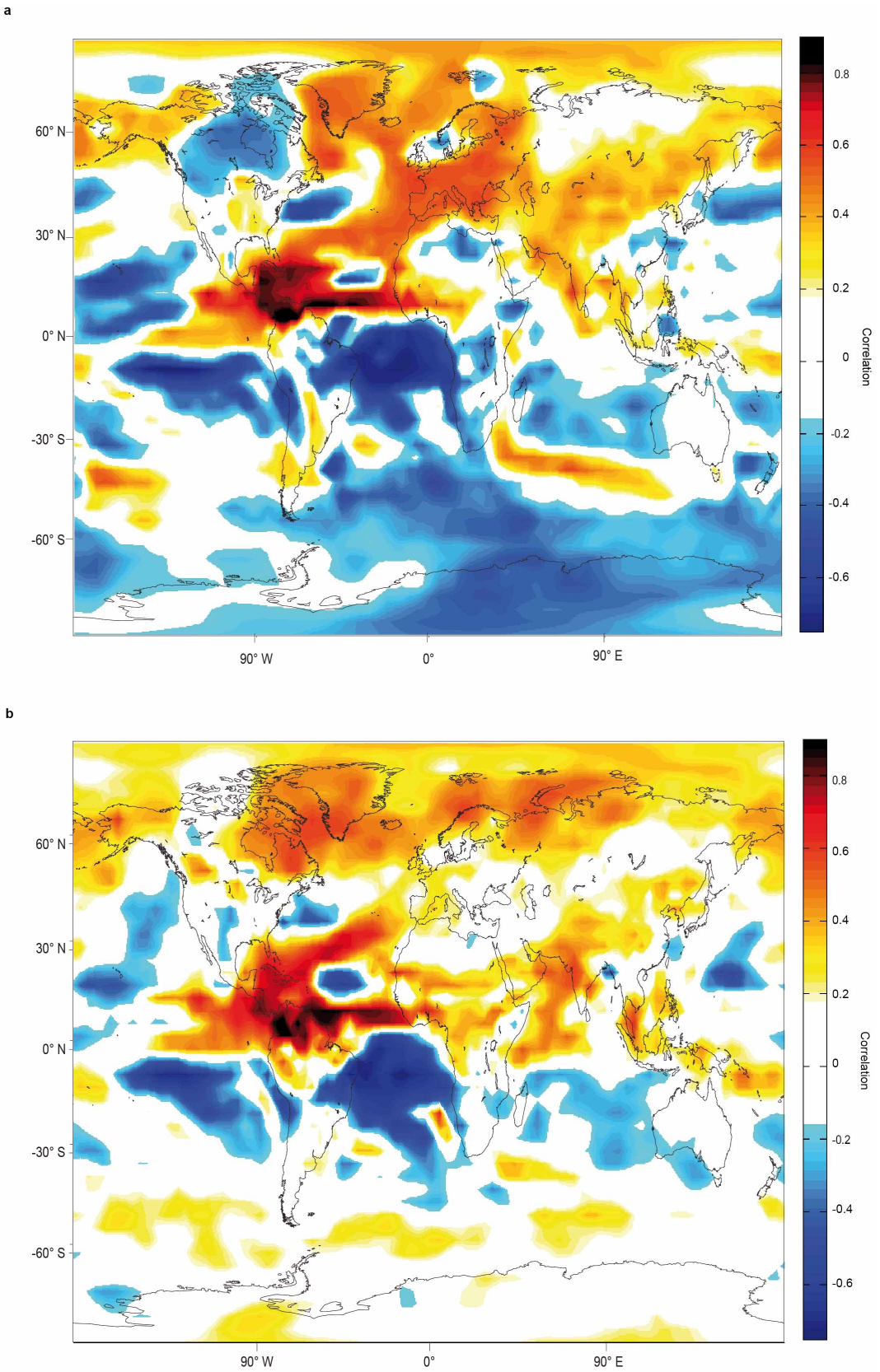

Extended Data Figure 5 | Decadal precipitation variations in the Ritacuba region (75–71° W, 2–6° N) correlated with global precipitation. **a**, Correlations during the ACR period. **b**, Correlations during the Younger Dryas period. Statistically insignificant ($P > 0.05$) values are shown in white.

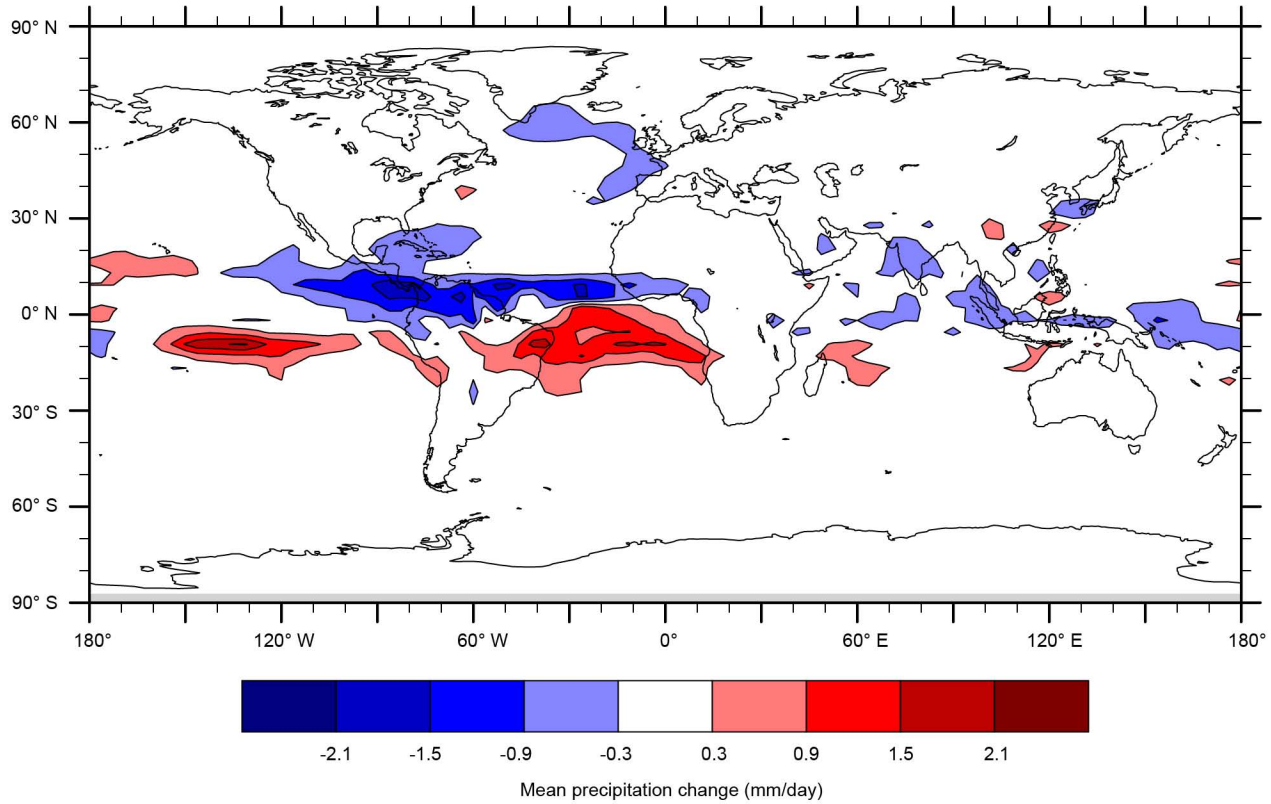

Extended Data Figure 6 | Mean precipitation change during the Younger Dryas. Data for 12.9 kyr ago minus data for 12.0 kyr ago.

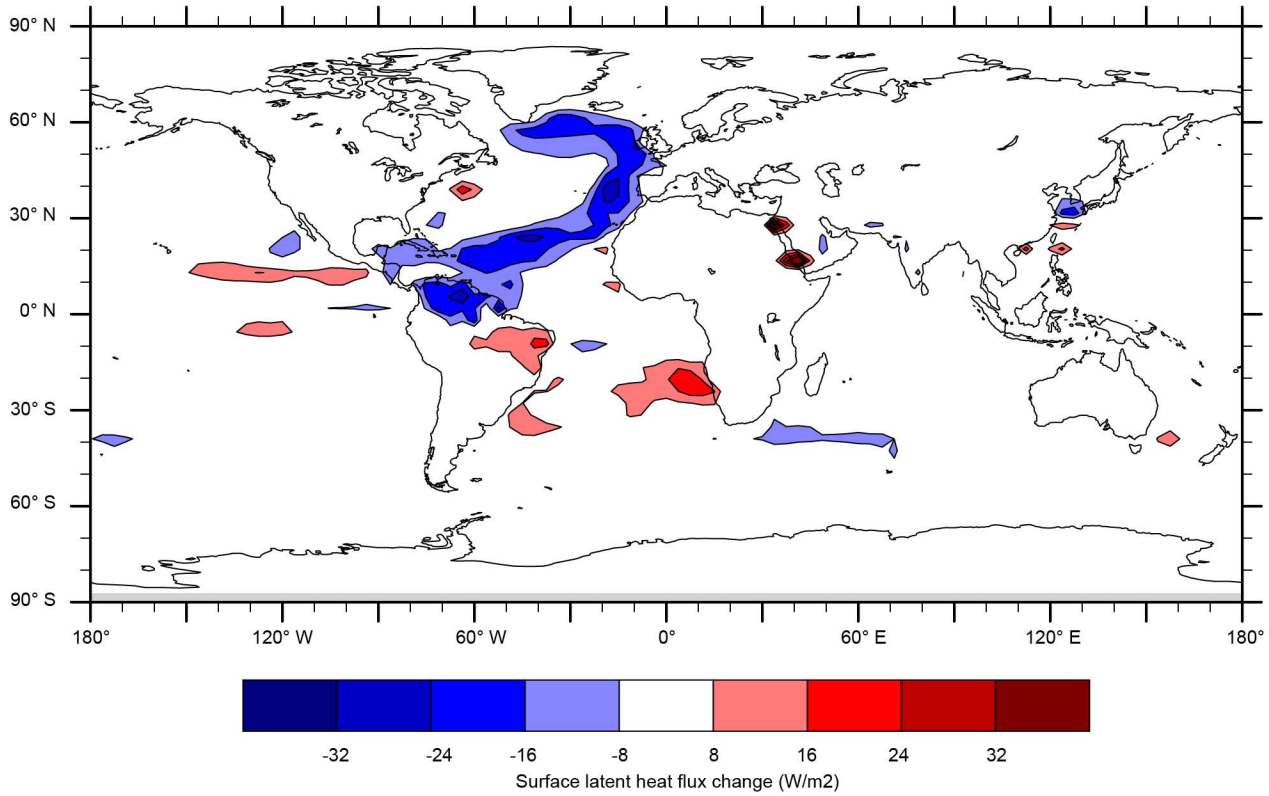

Extended Data Figure 7 | Latent heat change during the Younger Dryas. Data for 12.9 kyr ago minus data for 12.0 kyr ago.

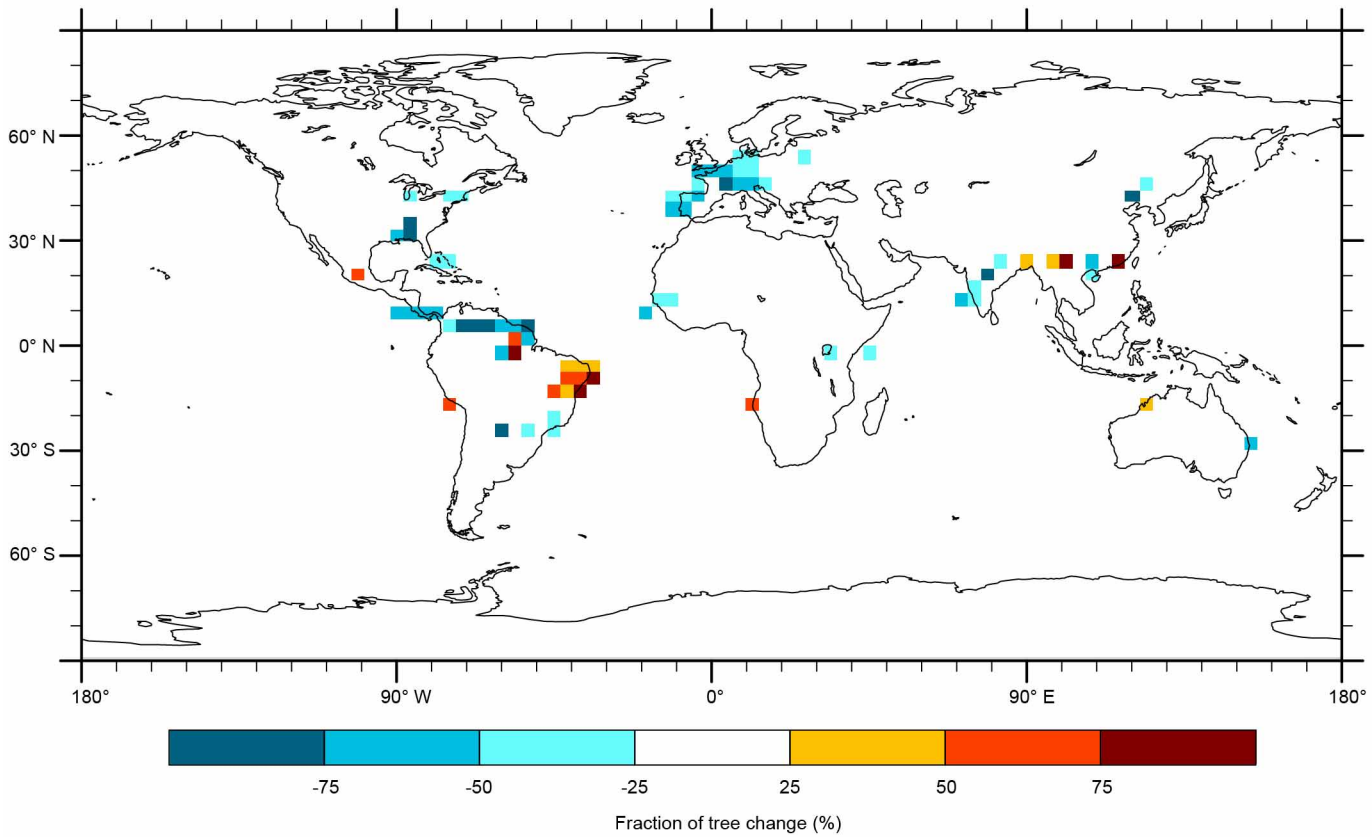

Extended Data Figure 8 | Simulated change in tree fraction during the Younger Dryas. Data for 12.9 kyr ago minus data for 12.0 kyr ago.

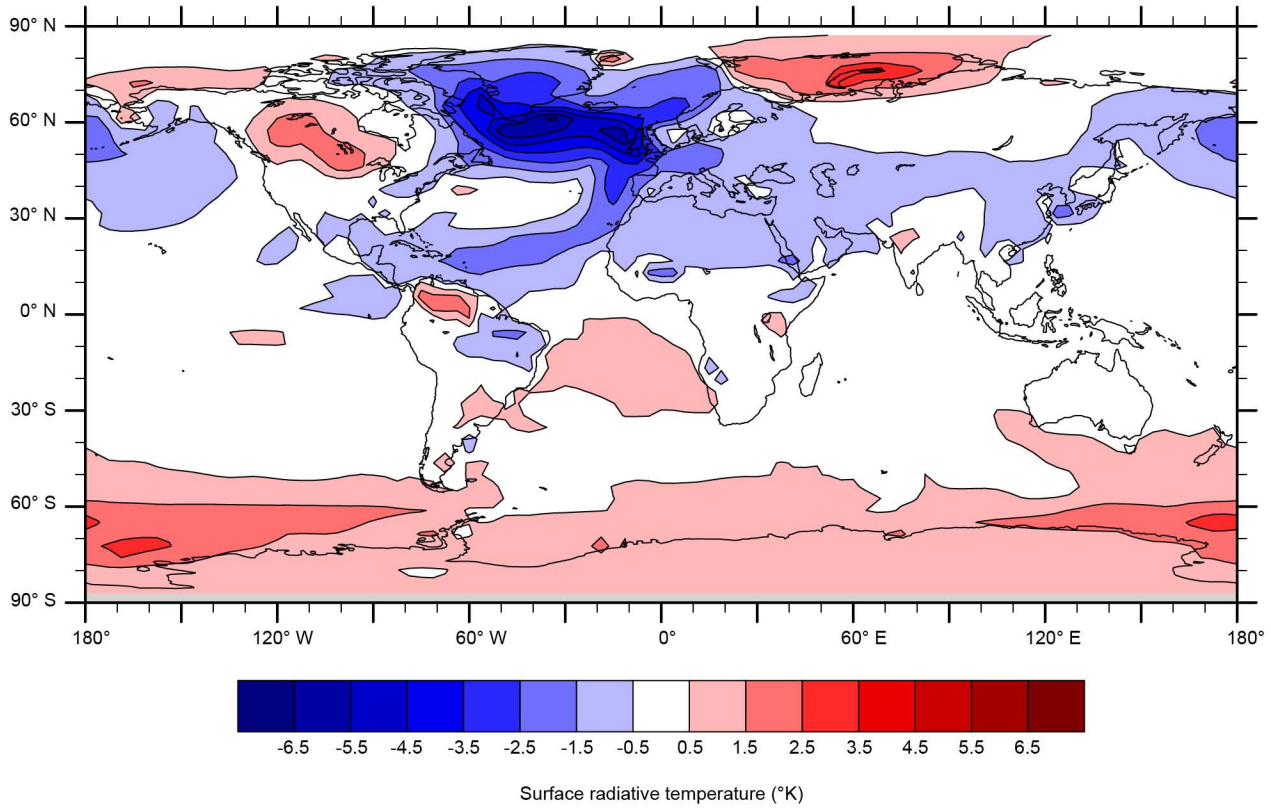

Extended Data Figure 9 | Surface temperature change during the Younger Dryas. Data for 12.9 kyr ago minus data for 12.0 kyr ago.